Computers & Geosciences 41 (2012) 88–98

Contents lists available at SciVerse ScienceDirect

Computers & Geosciences

journal homepage: www.elsevier.com/locate/cageo

A subwaveform threshold retracker for ERS-1 altimetry: A case study in the Antarctic Ocean

Yuande Yang [a,b], Cheinway Hwang [b,*], Hung-Jui Hsu [b], Dongchen E[a], Haihong Wang [c]

[a] Chinese Antarctic Center of Surveying and Mapping, Wuhan University, 129 Luoyu Road, Wuhan 430079, China
[b] Department of Civil Engineering, National Chiao Tung University, 1001 Ta Hsueh Road, Hsinchu, Taiwan
[c] School of Geodesy and Geomatics, Wuhan University, 129 Luoyu Road, Wuhan 430079, China

ARTICLE INFO

Article history:
Received 23 December 2010
Received in revised form
19 August 2011
Accepted 19 August 2011
Available online 6 September 2011

Keywords:
Altimeter
Antarctic Ocean
Gravity anomaly
Retracker
Sea surface height
Subwaveform

ABSTRACT

Based on a correlation analysis method, a subwaveform threshold retracker is developed and coded in FORTRAN for satellite altimetry to determine the leading edge and retracking gate, and to improve the precision of sea surface heights (SSHs) and gravity anomalies (GAs). Using ERS-1/ERM waveforms, the subwaveform threshold retracker outperforms full-waveform threshold retrackers at the tide gage Port Station. A direct comparison between retracked SSHs and in situ SSHs is made at tide gage Port Station. Here the subwaveform retracking improves SSH precision from 0.241 to 0.193 m, yielding an improvement percentage (IMP) of 20%. Using ERS-1/GM waveforms, the subwaveform threshold retracker outperforms the Beta-5 and full-waveform threshold retrackers over the Bellingshausen and Amundsen Seas (BAS) in the Antarctic Ocean. The standard deviations of raw and retracked SSHs are 0.157 and 0.070 and 1.836 and 0.220 m over the ice-free and ice-covered oceans, corresponding to IMPs of 54.4% and 88%, respectively. Use of retracking improves the precision of GAs by up to 46.6% when comparing altimeter-derived and shipborne GAs.

1. Introduction

Satellite altimetry has been widely used in many disciplines of Earth science. A summary of altimetric theories and applications is given by Fu and Cazenave (2001). For a pulse-limited radar, the return waveform is the basic measurement. The waveform is used to derive the range between the satellite antenna and the Earth's surface, which in turn yields surface topography at sea and land. Over oceans, the radar ranging accuracy can normally meet the mission-required accuracy due to the reflecting surface of the ocean that result in an ideal waveform, i.e., the Brown waveform (Brown, 1977; Sandwell and Smith, 2005). The ranging accuracy is quickly degenerated as the observation is near coasts or over nonocean surfaces, largely due to waveform contamination (Deng, 2003; Deng et al., 2003; Deng and Featherstone, 2006; Hwang et al., 2006).

Over oceans, the waveform contamination can happen not only near coastal areas, but also over areas covered with sea ice. A postprocessing technique, known as waveform retracking, can be used to retrack the corrupted waveform and in turn improve the ranging accuracy of altimeter-derived sea surface height (SSH). For geodetic and geophysical applications, SSHs from altimetry are often used to derive gravity anomalies (GAs). For example, Brooks et al. (1997), Sandwell and Smith (2005), Deng and Featherstone (2006), Hwang et al. (2006), and Sandwell and Smith (2009) show that waveform retracking can improve the accuracies of SSHs and GAs over both open and shallow waters.

Several algorithms have been developed to retrack waveforms over different reflecting surfaces, such as land/sea ice, land, and coastal waters (Gommenginger et al., 2011). For example, the Beta retracker (Martin et al., 1983), the threshold retracker (Wingham et al., 1986), and the surface/volume retracker (Davis, 1993) have been used over ice. A review of waveform retracking methods for different reflecting surfaces can be found in Deng and Featherstone (2006). These algorithms are based on either a statistical model or a deterministic model.

This paper presents a subwaveform retracker to compute range corrections for satellite altimetry. A FORTRAN computer program is developed to implement this retracker. This retracker first identifies the leading edge based on subwaveform correlation analysis, and then computes the retracking gate using a threshold method. This retracker will be compared with the Beta-5 and threshold retrackers to assess its performance in the Antarctic Ocean. Improvements in SSHs and GAs due to retracking by this method will be presented.

* Corresponding author.
E-mail addresses: cheinway@mail.nctu.edu.tw, cheinway@gmail.com (C. Hwang).
URL: http://www.space.cv.nctu.edu.tw (C. Hwang).

0098-3004/$ - see front matter © 2011 Elsevier Ltd. All rights reserved.
doi:10.1016/j.cageo.2011.08.017

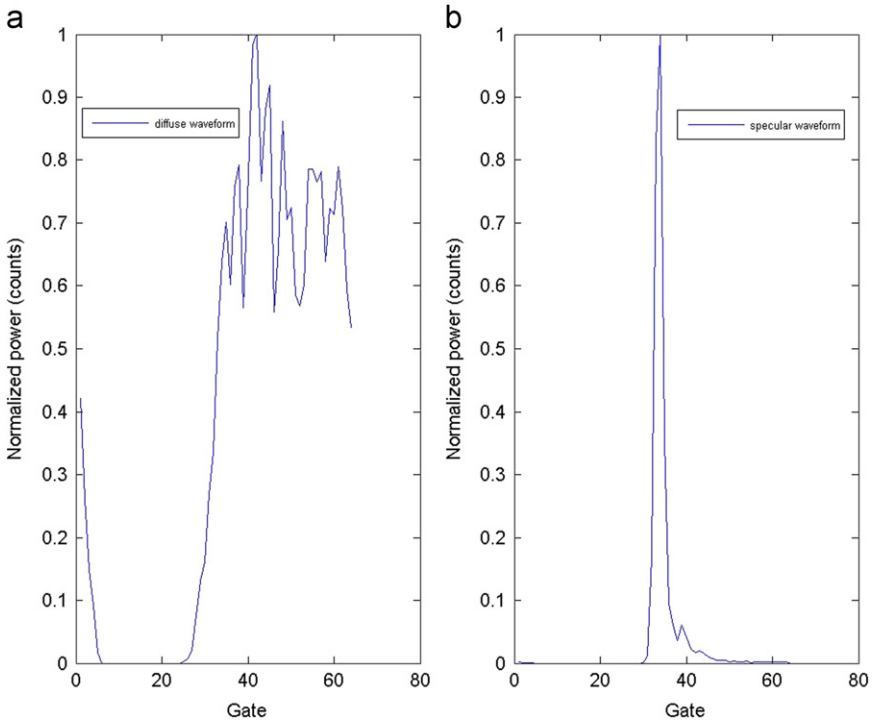

Fig. 1. A typical diffuse waveform (left) and a specular waveform over an ice-covered oceanic surface in the Antarctic Ocean.

2. Algorithm for leading edge determination and retracking

2.1. Diffuse and specular waveforms

Since our case study will be carried out in the Antarctic Ocean, a waveform classification is presented here. A waveform can be specular over an ice-covered ocean and diffuse over an ice-free ocean. A specular waveform is characterized by an initial sharp rise, followed by a rapid fall off in power. For a diffuse waveform, the rise of the leading edge and the trailing edge depends largely on a significant wave height (SWH). Fig. 1 shows a typical specular waveform and a typical diffuse waveform of ERS-1. The peak power of a specular waveform can be up to 3 orders of magnitude greater than that of a diffuse waveform (Laxon, 1994; Peacock and Laxon, 2004). A waveform classification is to distinguish specular waveforms from diffuse ones. In the classification, the pulse peakiness (PP) is computed as (Peacock and Laxon, 2004; Lee, 2008)

$$\mathrm{PP} = \frac{31.5 \times P_{max}}{\sum_{i=5}^{64} P(i)}, \tag{1}$$

where P_{max} is the waveform peak power, and $P(i)$ is the power of the ith gate. A waveform with $\mathrm{PP} < 1.8$ is regarded as a diffuse waveform (Peacock and Laxon, 2004); otherwise it is a specular one. Over oceans, this classification can be used to distinguish the ice-free area from the ice-covered area; see the case study in Section 4.

2.2. Brown waveform model and waveform correlation

The return power of a Brown waveform, $P(t)$, can be expressed as (Brown, 1977; Sandwell and Smith, 2005)

$$P(t) = \frac{A}{2}\left[\mathrm{erf}\left(\frac{t-\tau}{\sqrt{2}\sigma}\right)+1\right]\begin{cases} 1 & t<\tau \\ \exp(-(t-\tau)/\alpha) & t \geq \tau \end{cases}, \tag{2}$$

where A is the amplitude of the power, σ is associated with the slope of the leading edge governed by SWH, t is the time of gate, τ is the center of the leading edge, α is an exponential decay parameter in the trailing edge, and erf is the error function. For the ERS-1 waveform, α can be regarded as a constant (137 ns) (Sandwell and Smith, 2005). Therefore, the parameters A, τ, and σ govern the shape of the waveform. The rise width σ is a convolution of the effective width of the point target response and the vertical distribution of ocean surface waves, usually parameterized in terms of SWH. For a theoretical ERS-1 waveform, τ is 32.5 in dimensionless unit of sample gate width and can be converted to time by 3.03 ns (Fu and Cazenave, 2001). Therefore, a waveform shape with $A=1$ is determined by the parameter σ.

Correlation is a statistical method used to describe the dependence between two observed arrays. This method is adapted to analyze the relationship between two waveforms. A correlation coefficient is computed as

$$r = \frac{S_{r'r}}{\sqrt{S_{r'}S_r}}, \tag{3}$$

with

$$S_{r'} = \frac{1}{k-1}\sum_{i=1}^{k}(P_{r'}(i)-\overline{P_{r'}})^2, \tag{4}$$

$$S_r = \frac{1}{k-1}\sum_{i=1}^{k}(P_r(i)-\overline{P_r})^2, \tag{5}$$

$$S_{r'r} = \frac{1}{k-1}\sum_{i=1}^{k}(P_{r'}(i)-\overline{P_{r'}})(P_r(i)-\overline{P_r}), \tag{6}$$

where $P_{r'}(i)$ and $P_r(i)$, $i=1, \ldots, k$ are the return powers of the reference waveform and an arbitrary waveform, respectively, $\overline{P_{r'}}$ and $\overline{P_r}$ are the average powers, $S_{r'}$ and S_r are the standard deviations of the powers, and $S_{r'r}$ is the covariance of the two time series of powers from the reference and arbitrary waveforms. For an ERS-1 waveform, k is 64. A waveform is composed of thermal noise, leading edge, and trailing edge. In these three parts, the samples of the leading edge are more accurate than the other

parts. The sharp increase of return power in Fig. 1 corresponds to the leading edge of the waveform. This leading edge is over a subwaveform of this full waveform. The objective of our analysis is to derive the leading edge to reduce the error in the estimated arrival time of the pulse, hence to improve the precision of SSHs and GAs. This is achieved in four steps. The first is to obtain an accurate reference leading edge from the Brown model. Then, the subwaveform correlation is used to derive the optimal subwaveform. Third, the leading edge is determined after analyzing the optimal subwaveform. Finally, the retracking correction is derived from the leading edge with the threshold retracking.

2.3. Determining the leading edge by matching with a reference subwaveform

The determination the leading edge of a waveform is critical to the correlation method. Two experiments are done with theoretical ERS-1 waveform data from the Brown model: experiment 'A' does the subwaveform correlation; experiment 'B' is to analyze the affect of τ on subwaveform correlation. Fig. 2 shows the theoretical waveforms of ERS-1 based on Eq. (2), with SWHs ranging from 1 to 19 m at a 2-m interval. The slope of the leading edge increases with decreasing SWH. In the extreme case of SWH=0 over an ice-covered ocean, the waveform becomes specular (see Fig. 1).

In experiment 'A', we show the correlation coefficient (CC) between a reference subwaveform and an arbitrary subwaveform as follows. The reference subwaveform contains theoretical return powers of the ERS-1 altimeter from gate 20 to gate 42 (22 return powers), based on SWH=5 m. This subwaveform covers the leading edge of the waveform. For all the waveforms given in Fig. 2, the CC between the reference subwaveform and a moving subwaveform is computed. A moving subwaveform contains 22 return powers. For ERS-1, a waveform contains 43 such subwaveforms, resulting in 43 CCs. Fig. 3 shows the CCs for all the waveforms in Fig. 2. The largest and the smallest CCs (excluding the case SWH=5 m) occur in the cases of SWH=7 and 19 m, and they are 0.997 and 0.949, respectively. This shows high correlations among the subwaveforms of different SWHs. The largest CC corresponds to the optimal subwaveform, which covers the leading edge or is just part of the leading edge. This indicates that waveform correlation can be used to determine the optimal subwaveform. Also, for the theoretical waveforms in Fig. 2, the largest CC occurs at gates between 18 and 21, depending on SWH, and the CC turns from positive to negative at gates between 32 and 34 (this gate is called the zero crossing gate).

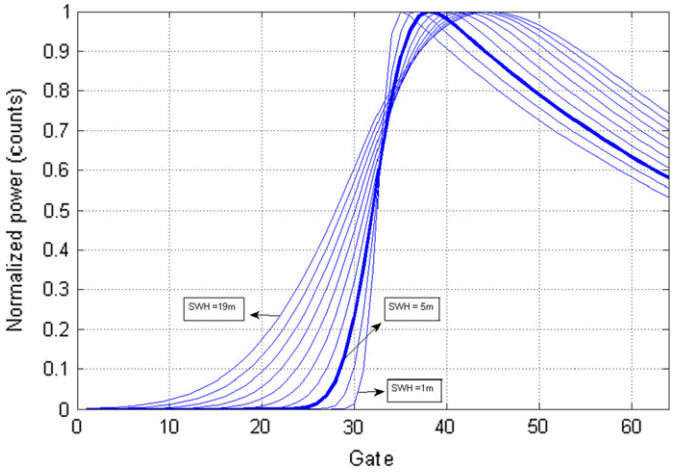

Fig. 2. Theoretical waveforms with SWH from 1 to 19 m. The waveform in blue is based on SWH=5 m, and its subwaveform over gates from 20 to 42 is the reference subwaveform.

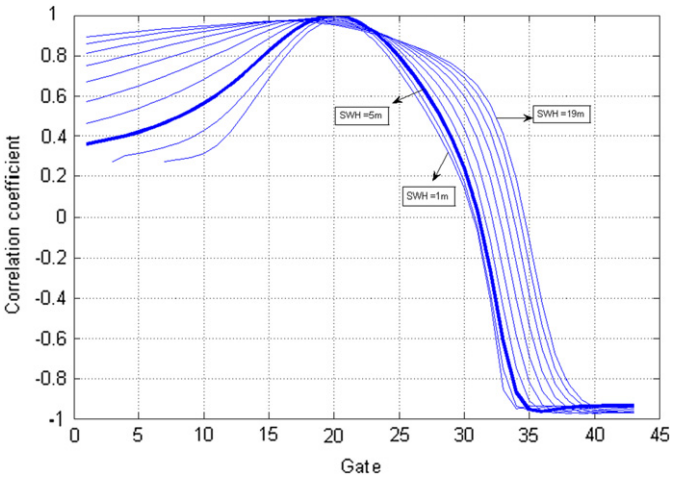

Fig. 3. Correlation coefficients between the reference subwaveform and the subwaveforms of varying SWH (including SWH=5 m).

Affected by several factors such as SWH and radar measurement noise, τ can be different from 32.5. In experiment 'B', the theoretical waveforms of ERS-1 are based on Eq. (2), with τ ranging from 28.5 to 36.5 at a 1-s interval and SWH=5 m. The CCs between the reference subwaveform and a moving subwaveform are computed. The reference subwaveform is the same as that used in experiment A, with τ=32.5. The maximal CC (excluding the case τ=32.5) is almost 1 and occurs at gates between 16 and 24. When τ increases by 1, the gate of maximal CC also increases by 1. Hence the CC can reflect the change of τ.

However, for an observed waveform of ERS-1, the CCs can be different from the ideal values given in Fig. 3. The reason is that the shape of the waveform (for both diffuse and specular waveforms) can deviate from the ideal shape following Eq. (2). For example, Fig. 4 shows the CCs between the reference subwaveform (same as the one used in Fig. 2) and the 43 subwaveforms of an observed diffuse and an observed specular waveform over the Antarctic Ocean. For the diffuse waveform (Fig. 4a), the maximal CC is about 1 and occurs at gate=19, around which the CCs fluctuate rapidly. The zero crossing gate is 32. For the specular waveform (Fig. 4b), the maximal CC is about 0.55 and occurs at gate=17, with the zero crossing gate at 22. The variation of CC in the case of the specular waveform is also quite irregular.

In fact, the optimal subwaveform is not always the same as the leading edge. The first and the last gates of the leading edge are determined using an algorithm given in Fig. 5. In Fig. 5, i_{max} is the gate corresponding to the maximal CC, i_c is the gate of zero crossing, and $\Delta_i = i_c - i_{max}$ is the gate difference. In general, the gate difference increases with SWH. Since the reference subwaveform is based on SWH=5 m, the ideal gate difference is 12. Thus, if the gate difference is 12, the leading edge of the observed subwaveform contains 22 samples as in the reference subwaveform. If the gate difference is not 12, an empirical method, detailed in Fig. 5, was used to select the first and the last gates of the leading edge. The leading edge contains the return powers from gate i_{first} to i_{last}. We must stress that, although the reference subwaveform is based on Eq. (2), our algorithm of the leading edge identification is effective for both specular and diffuse waveforms. Also, if an observed waveform contains multiple ramps, the subwaveform identified by the method presented in this section is again the optimal one; see also Section 4 for the assessments.

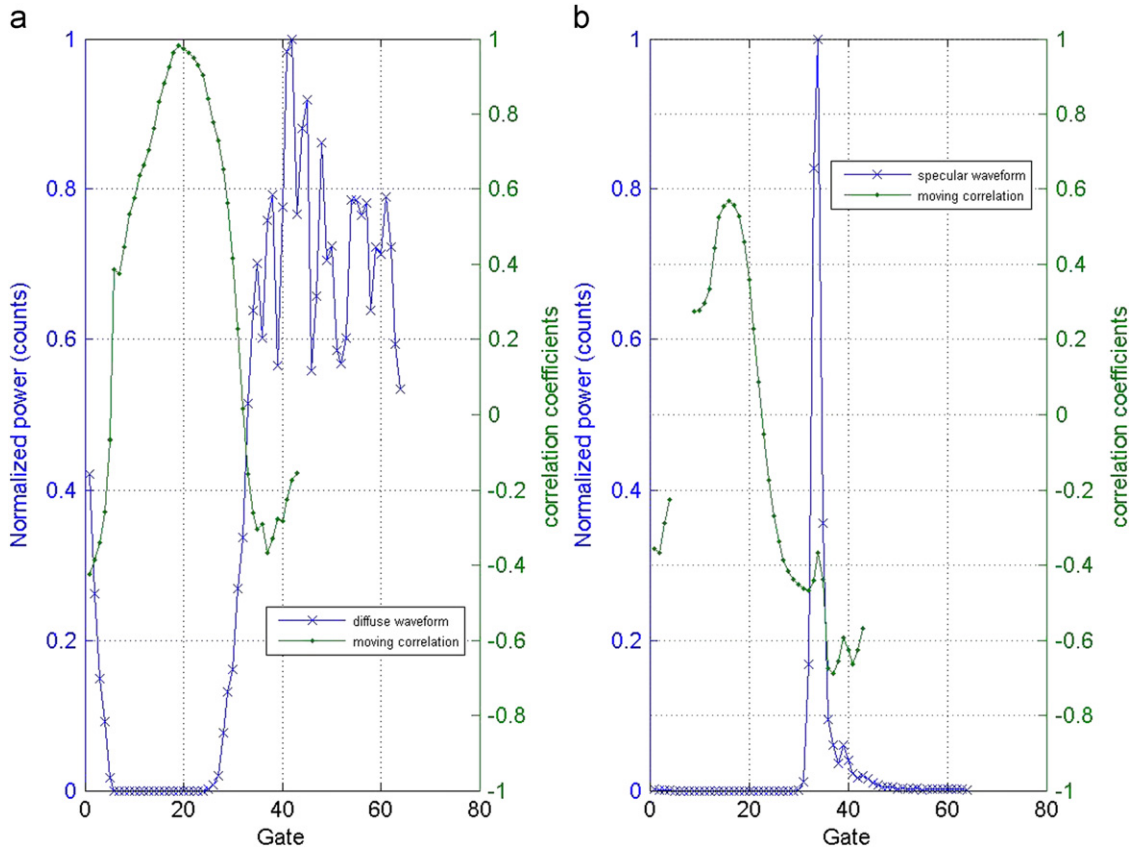

Fig. 4. Correlation coefficients between the reference subwaveform and the 43 subwaveforms for an observed diffuse waveform and an observed specular waveform.

2.4. Retracking the leading edge using threshold retracker

Once the leading edge is identified, the retracking gate, which must fall within this subwaveform, is determined by the threshold retracking (Davis, 1997). This method computes retracking gate using the formulas

$$A = \sqrt{\sum_{i=1}^{i_{sample}} P_i^4(t) / \sum_{i=1}^{i_{sample}} P_i^2(t)}, \tag{7}$$

$$P_N = \frac{1}{5}\sum_{i=1}^{5} P_i, \tag{8}$$

$$T_l = (A - P_N)\cdot \mathrm{Th} + P_N, \tag{9}$$

$$G_r = G_{k-1} + (G_k - G_{k-1})\frac{T_l - P_{k-1}}{P_k - P_{k-1}} + i_{first}, \tag{10}$$

where i_{sample} is the number gates of the leading edge, A is the amplitude of the leading edge, $P_i(t)$ is the normalized power of waveform at the ith gate, P_N is the averaged value of the first five normalized powers, Th is a threshold value, G_k is the kth gate whose normalized power is greater than T_l, G_r is the retracking gate.

Note that if P_k equals P_{k-1}, then k is replaced by $k+1$. The range correction is then computed by

$$C = (G_r - G_T)\Delta R, \tag{11}$$

where G_T is the theoretical retracking gate and ΔR is the range corresponding to one gate. The method for computing A is the same as the method for the OCOG retracking (Appendix A). For the ERS-1 altimeter, $G_T = 32.5$, and $\Delta R = 0.4545$ m. The optimal threshold value is obtained using certain criterion and this is discussed in Section 4.

3. A FORTRAN program for leading edge determination and retracking

A FORTRAN program, called subwave.f, was developed to implement the theory of subwaveform threshold retracking. This program first computes CCs between the reference waveform (cf. Fig. 2) and the subwaveforms of a full waveform (containing all return powers) to determine the leading edge for retracking. The retracking gate of this subwaveform is then determined by the threshold retracking (Section 2.3, but using only return powers within the leading edge). The computer program also includes the Beta-5 and OCOG retrackers (the methods are given in Appendix A) and the full-waveform threshold retracker. The full-waveform threshold retracker in subwave.f uses the full waveform and its theory is given in Section 2.3. This program accepts command-line arguments and operates in the UNIX and the Microsoft DOS environment. The usage of this program, which also appears as comments in the program, is presented below

NAME

subwave: program to compute the centers of leading edge or retracking corrections of waveform using subwaveform threshold retracking, Beta-5, OCOG, and full-waveform threshold retracking

SYNOPSIS

subwave –Fwaveform_file -Gofile2 [-Tretracker -Odata_type -Hthreshold_value -Cofile1]

- -F: this input file contains return powers of waveform
- -G: this output file contains retracking corrections (or the centers of leading edge)

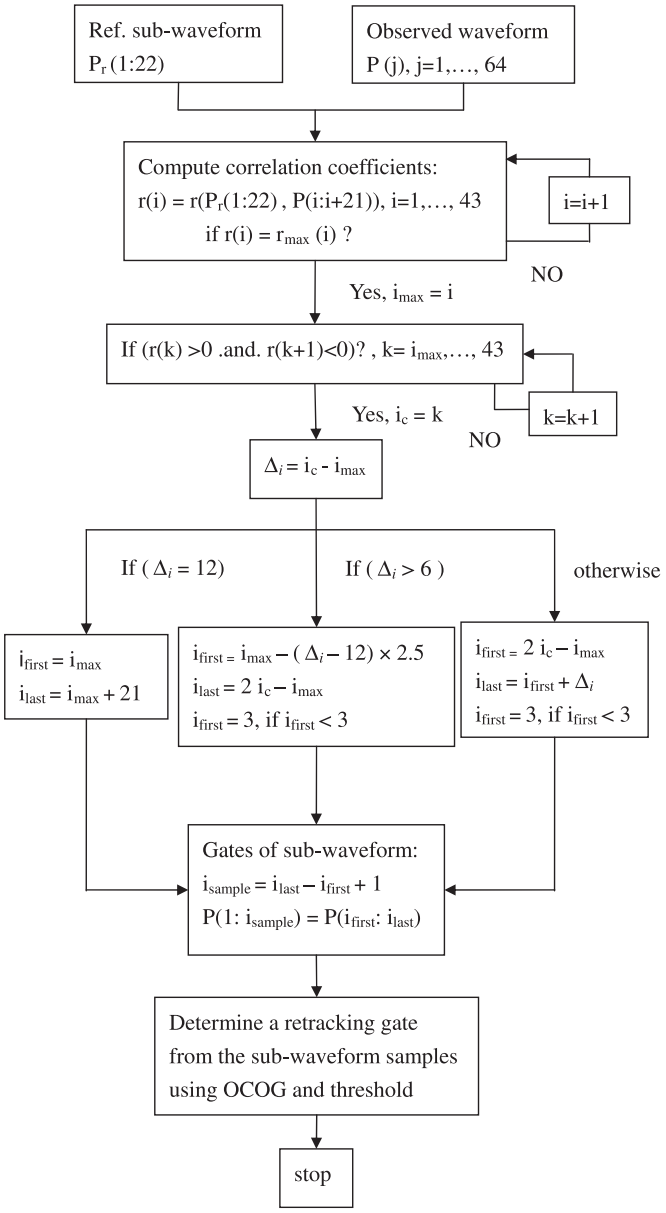

Fig. 5. Alogrithm for determining the gates of the optimal subwaveform.

OPTIONS

– -T: retracker=1: subwaveform threshold retracker (default)
retracker=2: Beta-5 retracker
retracker=3: OCOG retracker
retracker=4: full-waveform threshold retracker

-O: type of output
type=1: retracking corrections (default)
type=2: the center of the leading edge

-H: threshold value for threshold retracking (subwaveform or full waveform)
-C: this output file contains the correlation coefficients of 43 subsets for each full waveform

Each record of waveform in the input file (-F) contains latitude, longitude, and 64 return powers. This file can be easily modified to adopt waveforms other than ERS-1s. Note that the Beta-5, OCOG, and full-waveform retrackers determine the range corrections using the full waveform, in contrast to the subwaveform retracker which uses only the return powers within the leading edge (the number of powers used depends on SWH and is detailed in Fig. 5).

4. A case study in the Antarctic Ocean

4.1. The waveform data of ERS-1 and the study area

We assessed the subwaveform retracker using ERS-1 altimeter data. ERS-1 is the first European Remote Sensing Mission, launched on 17 July 1991 and ended in 1996, with a 98.5° inclination angle at an altitude between 782 and 785 km. ERS-1/GM data were collected during two 168-day geodetic phases, and the cross-track spacing is 8 km at the equator. The ERS-1/ERM data were collected during the repeat phase after the geodetic phases. The ERS-1 altimeter transmits radar pulses at a frequency of 1020 Hz, and the onboard processor averages 50 return echoes to generate 20 sets of waveforms in 1 s. This results in the 20 Hz waveforms and subsequently the 20-Hz SSHs. Each set of waveforms contains 64 return powers. The geophysical corrections for the ERS-1 instantaneous SSHs include solid-Earth, pole and ocean tides, tropospheric and ionospheric corrections, inverse barometer effect, sea state bias, and ocean tides based on NAO99b (Matsumoto et al., 2000).

Our experiments were carried out over two areas around the Antarctic Ocean, one bounded by 55°S < latitude < 82°S, 225°E < longitude < 270°E, and the other by 51°S < latitude < 52°S, 301°E < longitude < 303°E. The first area is one of the world's southernmost seas, including a large portion of Bellingshausen and Amundsen Seas (BAS) lying offshore in West Antarctica. An accurate, high-resolution gravity field over BAS from satellite altimetry can reveal important details about the tectonic history of this region, such as the plate tectonic behavior since 18 Ma of West Antarctica and the Campbell Plateau—New Zealand microcontinent (McAdoo and Laxon, 1997). Moreover, some parts of BAS are covered with perpetual and seasonal sea ice. Due to varying surface reflecting properties, BAS is an ideal region to test different waveform retrackers. The tide gage Port Station, shown in Fig. 6, is located at 51.45°S, 302.0667°E in the second area. Here selected tidal records will be used to assess the performances of different retrackers.

4.2. Direct assessment using tide gage data

The range correction from retracking can be used to compute improved SSH, which is called retracked SSH below. There are many methods for assessing the quality of retracked SSH, e.g., analysis of crossover differences of SSH and comparison between retracked SSH with a well-defined field. In the Antarctic Ocean, crossover points may be sparse and interrupted by sea ice, and the crossover differences of SSH can be easily amplified by spurious SSH (even with retracking).

As a direct method of quality assessment, we compared retracked SSHs with hourly tidal records at Port Station gage data from University of Hawaii Sea Level Center (UHSLC, http://ilikai.soest.hawaii.edu/uhslc/datai.html) over 1992 to 2011. The closest subsatellite point of ERS-1/ERM is about 3 km from Port Station (Fig. 6). Only data from passes 19444, 19945, 20446, 20947, 21448, and 21949 of ERS-1/ERM are available for assessment near Port Station. Because the tide gage and altimetry records are not on the same vertical datum, the demeaned SSHs, named sea level anomalies (SLAs), from tide gage and altimetry near Port Station were compared; see also Fenoglio-Marc (2002). Affected by land mass near Port Station, Beta-5 fails to retrack most of the

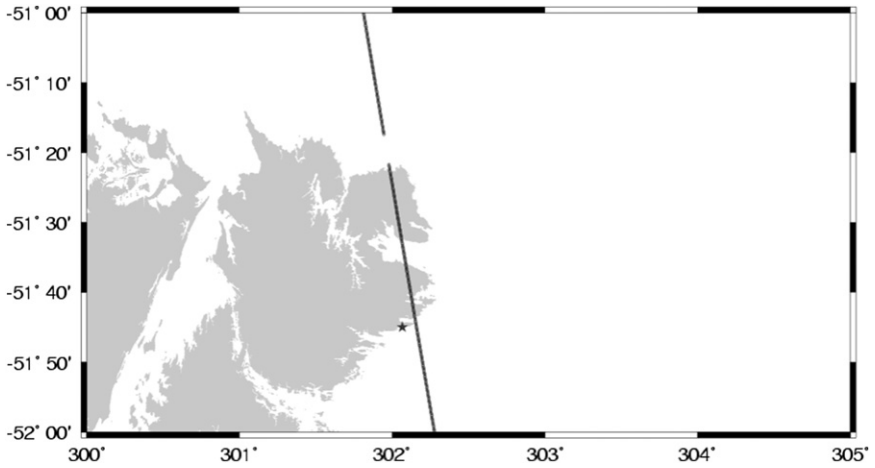

Fig. 6. Tide gage (star) and ground track of pass 19444 of ERS-1/ERM.

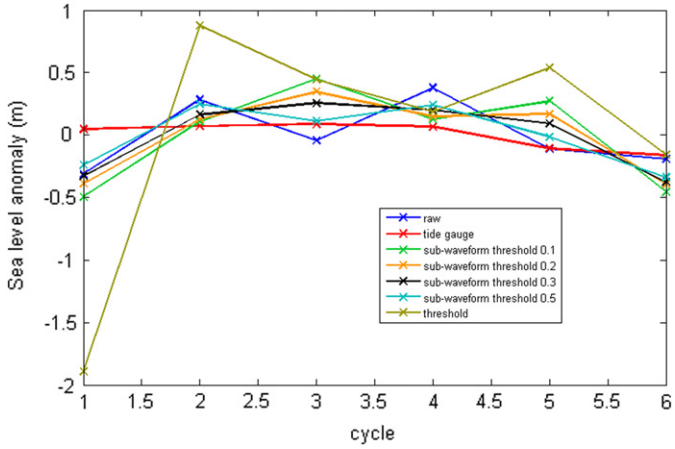

Fig. 7. Sea level anomalies at Port Station from tide gage, raw, and retracked ERS-1. Cycles 1–6 correspond to passes 19444, 19945, 20446, 20947, 21448, and 21949 of ERS-1/ERM.

Table 1
Statistics of differenced SSH (in m) between ERS-1 and tide gage.

Altimeter SSHs	Mean	Standard deviation
Raw	0.605	0.241
Subwaveform threshold 0.1	0.850	0.364
Subwaveform threshold 0.2	0.571	0.284
Subwaveform threshold 0.3	0.392	0.239
Subwaveform threshold 0.5	0.075	0.193
Threshold[a]	−0.244	0.998

[a] Full waveform is used.

Table 2
Standard deviations of differenced SSHs (in m) along ERS-1 pass 14501 over BAS.

Ocean	Beta-5	Threshold[a]	Subwaveform threshold			
			0.1	0.2	0.3	0.5
Ice-free	0.100	0.100	0.059	0.062	0.067	0.088
Ice-covered	NA	0.404	0.192	0.229	0.261	0.368

[a] Full waveform is used.

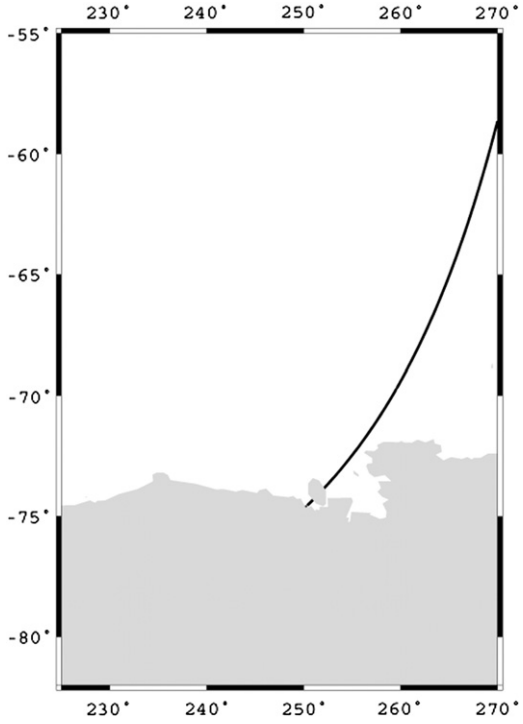

Fig. 8. Ground track of pass 14501 of ERS-1/GM over the Antarctic Ocean.

waveforms and the corresponding result is not shown in this assessment. Fig. 7 compares the raw and retracked SSHs near Port Station. Table 1 shows the statistics of the differences between tide gage- and ERS-1-derived SSHs. Table 1 suggests that retracking cannot always reduce the differences between tide gage- and ERS-1-derived SSHs around a coastal station such as Port Station, where waveforms can be seriously corrupted by land mass. However, the subwaveform threshold retrackers (with different threshold values) always outperform the full waveform threshold retracker. The comparison in Table 1 suggests that a threshold value of 0.5 is the optimal value for the subwaveform threshold retracker. The use of retracked SSHs reduces the standard

deviation of the SSH differences from 0.241 to 0.193 m, yielding an improvement percentage (IMP) of 20%. IMP is the ratio between the difference of the standard deviations of the raw and retracked SSHs and the standard deviation of the raw SSHs (Hwang et al., 2006). The mean difference is also reduced from 0.605 to 0.075 m by retracking.

Table 3
Standard deviations of differenced SSHs (in m) over BAS.

Ocean	Beta-5	Threshold[a]	Subwaveform threshold			
			0.1	0.2	0.3	0.5
Ice-free	0.118	0.124	0.070	0.074	0.083	0.110
Ice-covered	NA	0.349	0.220	0.232	0.253	0.322

[a] Full waveform is used.

Table 4
Statistics of range corrections (in m) from the subwaveform retracker.

Ocean	Max	Min	Mean	Standard deviation
Ice-free	5.844	−7.236	−0.003	0.233
Ice-covered	10.688	−12.131	0.094	1.646

4.3. Indirect assessment using along-track differenced residual SSH

In this section, we use an indirect quality assessment of retracked SSHs as follows. We first computed the difference between the retracked SSH and the geoidal height from the EGM2008 geopotential model (Pavlis et al., 2008), called residual SSH, as

$$N_{res} = N - N_{long}, \tag{12}$$

where N_{long} is the geoidal height from EGM2008 using the all-harmonic coefficients provided by the EGM2008 (complete to spherical harmonic degree and order 2159, and contains additional coefficients extending to degree 2190 and order 2159). Furthermore, to reduce the effect of the ocean dynamic height and the long wavelength error in the altimeter ranging, we computed the differenced residual SSH between two successive points along satellite ground tracks as

$$\Delta N_{res} = N_{res2} - N_{res1}, \tag{13}$$

where N_{res1} and N_{res2} are two successive residual SSHs. The standard deviation of ΔN_{res}, denoted as $S_{\Delta N}$, over the interested area was then computed to serve as the descriptor of the improvement of SSH due to retracking. It is clear that $S_{\Delta N}$ will decrease with improved SSHs.

As an example, Table 2 compares $S_{\Delta N}$ values for different retrackers along ERS-1/GM pass 14501 (Fig. 8). Table 2 shows that the subwaveform threshold retracker outperforms the Beta-5 and the full-waveform threshold retrackers over both the ice-free

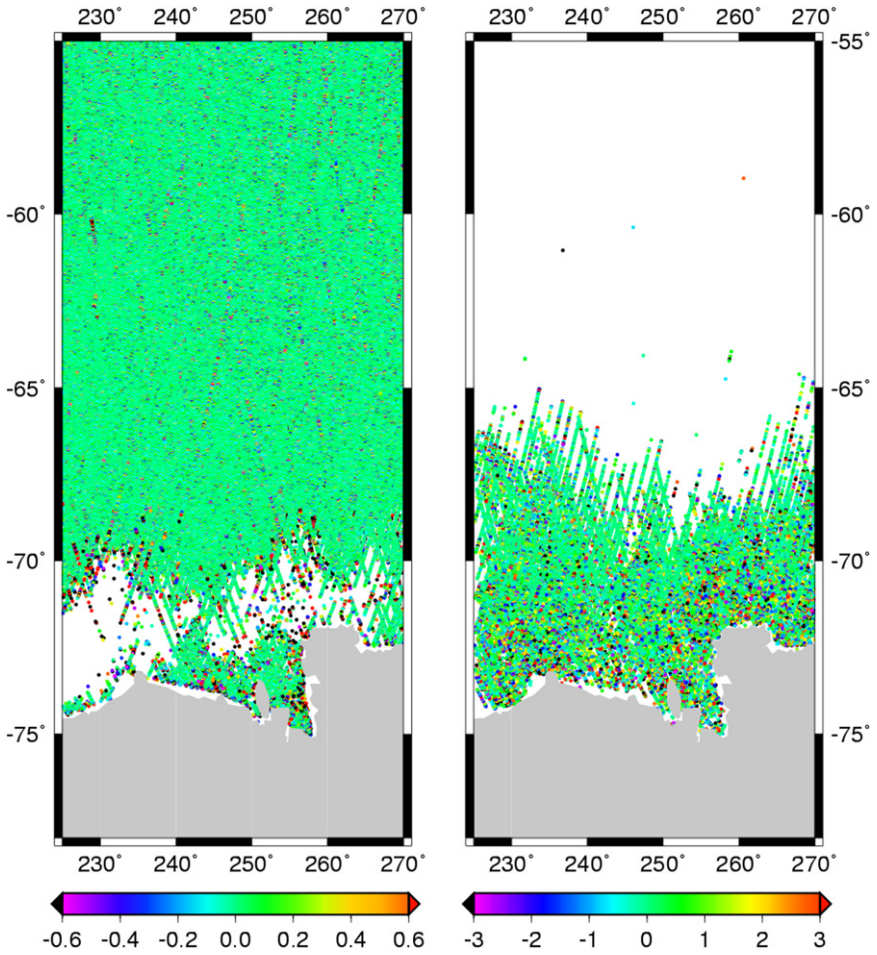

Fig. 9. Distribution of range corrections (in m) over (left) the ice-free ocean and the ice-covered ocean.

ocean and the ice-covered ocean. The optimal threshold value for the subwaveform threshold retracker was found to be 0.1, while for the full-waveform threshold retracker, the value was 0.5. The $S_{\Delta N}$ values from the subwaveform retracker (0.059 and 0.193 m over ice-free and ice-covered oceans, respectively) are about 50% of the $S_{\Delta N}$ from the full-waveform threshold retracker. The comparison in Table 2 suggests that the subwaveform retracker with a threshold value of 0.1 outperforms the other two retrackers. Also, the retracked SSHs over the ice-free ocean yield an $S_{\Delta N}$ that is about 25% of the $S_{\Delta N}$ over the ice-covered ocean. This indicates that retracked SSHs over the ice-free oceans are more accurate than those over the ice-covered ocean.

A further assessment was carried out over BAS using 2278 passes of ERS-1/GM. A comparison of the $S_{\Delta N}$ values from different retrackers is shown in Table 3. The results over BAS are similar to the result along pass 14501. Compared with pass 14501, the $S_{\Delta N}$ values of the subwaveform threshold retracker (again with 0.1 threshold value) over the ice-free and ice-covered oceans are 0.070 and 0.220 m, which are larger than that of pass 14501. The above two experiments (Tables 2 and 3) show that the subwaveform threshold retracker with a 0.1 threshold is the optimal retracker.

Table 4 shows the statistics of the range corrections from the subwaveform retracking over both the ice-free and ice-covered oceans. Table 4 suggests that the average range correction over the ice-covered ocean is much larger than that over the ice-free ocean (1.646 vs. 0.233 m in terms of standard deviation). Since

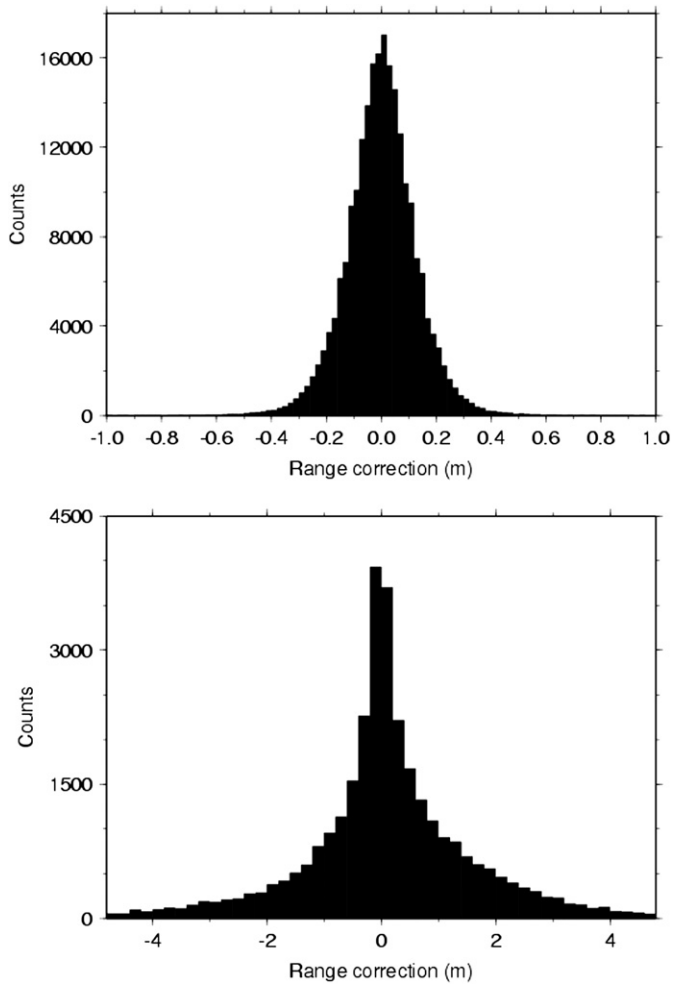

Fig. 10. Histograms of range corrections (in m) over the ice-free ocean (top) and the ice-covered ocean.

Table 5
Standard deviations of differenced SSHs from raw and retracked SSHs, and improvement percentage (IMP).

Ocean	Raw (m)	Retracked (m)	IMP (%)
Ice-free	0.157	0.070	55.4
Ice-covered	1.836	0.220	88.0

the ice-covered area of BAS is dominated by specular waveforms, here the range corrections are larger than those over the ice-free area, where diffuse waveforms are common. Fig. 9 shows the distribution of the range corrections over the two reflecting surfaces (ice-free vs. ice-covered). The average range correction over the ice-free ocean is smaller than that over the ice-covered ocean. There are some large corrections near the coasts (Deng and Featherstone, 2006). Furthermore, Fig. 10 shows the histograms of the range corrections over both surfaces. The histograms roughly follow the normal distribution.

Table 5 shows the IMP of SSH due to subwaveform retracking over BAS. In Table 5, the standard deviations of differenced residual SSHs from the raw SSH and from retracked SSH are compared. From Table 5, retracking has greatly improved the SSH accuracies over both surfaces. For example, the standard deviations over the ice-free ocean in the cases of the raw and the retracked SSHs are 0.157 and 0.070 m, respectively, and the improvement percentage is about 55.4%. Over the ice-covered ocean, the standard deviation is reduced from 1.836 to 0.220 m after retracking, yielding an IMP of 88%. Fig. 11 shows the distributions of differenced residual SSHs over the ice-covered ocean before and after retracking. In this case, retracking has again reduced the differenced residual SSHs and improve SSH. However, it is clear that not all SSHs can be properly corrected by retracking, and there still exist large differenced residual SSHs in Fig. 11. Possible causes of the large differenced residual SSHs in Fig. 11 are poor geophysical correction models and the fact that the sea ice surface is not identical to the ocean surface.

4.4. Improved gravity anomaly from retracked SSH

An indirect assessment of the retracked SSHs was also carried out: comparison between altimeter-derived GAs with shipborne GAs. We chose to use the inverse Vening Meinesz (IVM) formula (Hwang, 1998) to compute GAs from SSHs. For gravity derivation, the 20-Hz SSHs are resampled at a 2-Hz rate by a polynomial fitting and smoothing. Details of the resampling technique is given by Hwang et al. (2006). In the gravity derivation, along-track SSHs were first converted to geoid gradients, which were then used to create two $2' \times 2'$ grids of geoid gradients in the north–south and the west–east directions. The standard remove–restore procedure was applied in the gravity derivation, in which the EGM2008 using the all-harmonic coefficients provided by the model was adopted as the reference gravity field.

Two $2' \times 2'$ grids of GAs over BAS were derived, one from the retracked SSHs and another from the raw SSHs of ERS-1/GM. The shipborne GAs over BAS from the National Geophysical Data Center (NGDC) (http://www.ngdc.noaa.gov) were then compared with the altimeter-derived GAs. Before comparison, the bias and drift along any of the cruises of the NGDC shipborne GAs were removed by the method described in Hwang and Parsons (1995), and outliers were deleted using the three-sigma criterion. A shipborne GA was deleted if the difference between the shipborne GA and the altimeter-derived GA exceeds three times that of the sigma. Table 6 shows the statistics of the differences between the altimeter-derived and shipborne GAs. The use of retracked SSHs has reduced the standard deviation of the

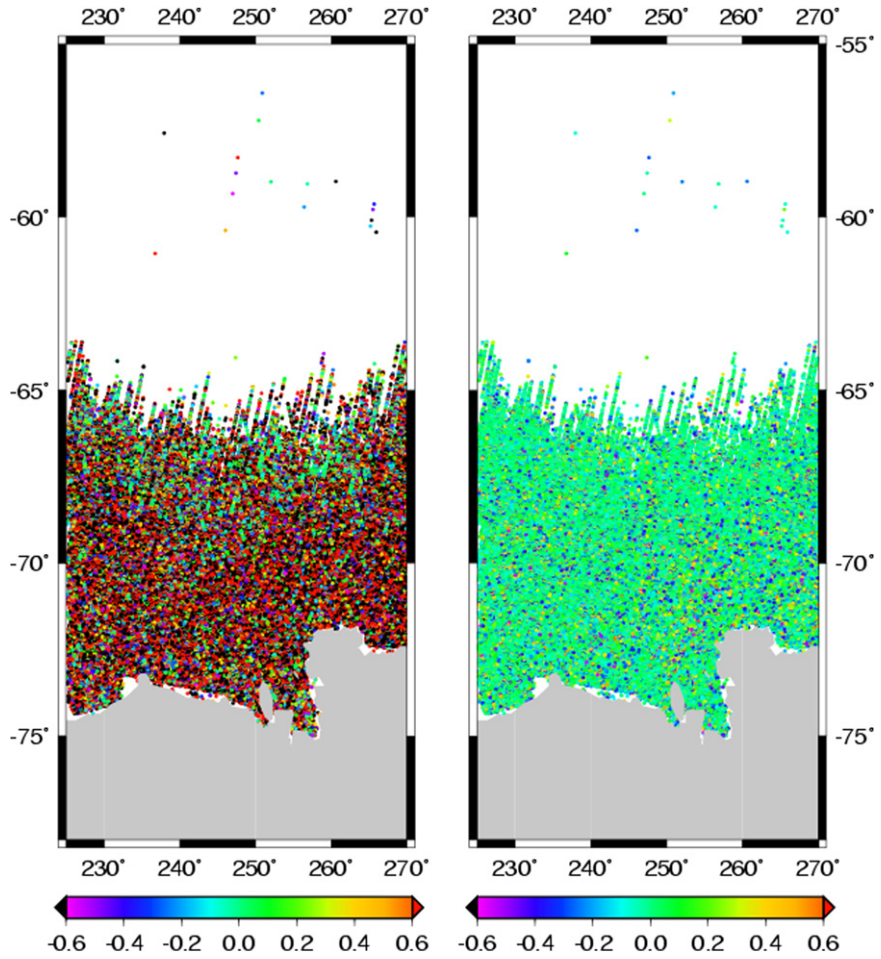

Fig. 11. Distributions of differenced residual SSH (in m) from specular waveforms before (left) and after retracking.

Table 6
Statistics of differences (in mgal) between altimeter-derived and shipborne gravity anomalies using raw and retracked SSHs.

SSH	Maximum	Minimum	Mean	Standard deviation
Raw	117.526	−81.525	1.052	15.038
Retracked	50.045	−47.567	0.147	8.028

differences from 15.038 to 8.028 mgal. The mean difference is also reduced due to retracking. In terms of standard deviation, the IMP due to the subwaveform retracking is 46.6%. Fig. 12 shows the distribution of the differences. The reduction of the differences due to retracking is evident in Fig. 12. In particular, the large differences over the ice-covered ocean have been significantly reduced due to the use of retracked SSHs.

5. Discussion and conclusions

The novel idea of the correlation method of retracking is matching a reference waveform (the ideal waveform, see Section 2.2) with selected sets of subwaveforms to determine the optimal subwaveform (also the leading edge) for retracking. Retracking over such a leading edge is found to produce the best improved SSH compared to the cases of using other subwaveforms. Our retracking is simply based on the threshold method that exists in the literature. Such a retracker is called subwaveform threshold retracker, which outperforms the full-waveform threshold and the Beta-5 retrackers. In addition to ERS-1, we expect that this retracker is applicable to waveforms from missions such as Geosat, TOPEX/Poseidon, ERS-2, Envisat, and Geosat-follow-on for best possible improved SSH. However, the optimal threshold values may vary with waveforms from different missions and with different applications, and selecting such values will be important for the success of this retracker. For example, the optimal threshold value for the subwave retracker in the direct assessment of tide gage records at Port Station is 0.5, while the optimal threshold value is 0.1 in the indirect assessments of residual SSHs and GAs.

The direct assessment of retracked SSHs at tide gage Port Station suggests that retracking can reduce the uncertainty of altimetry SSH by about 20%. Also, we use an "indirect" assessment of retracked SSH based on a comparison between altimeter-derived gravity and in situ shipborne gravity. Because SSH is essential to altimeter-derived gravity, the improvement in the former will naturally lead to the improvement in the latter. The assessment results show that retracking by the subwaveform threshold retracker improves the altimeter-derived gravity up to 46%.

It is important to understand that retracking alone cannot improve the quality of SSH. Retracking will only improve the ranging accuracy at short wavelengths (if the waveform is sufficiently good). Ranging accuracy at all wavelengths may be degraded by poor geophysical and environmental corrections. Finally, compared to the case over an ice-free sea surface, a more sophisticated data processing technique over an ice-covered sea surface is needed to obtain good results.

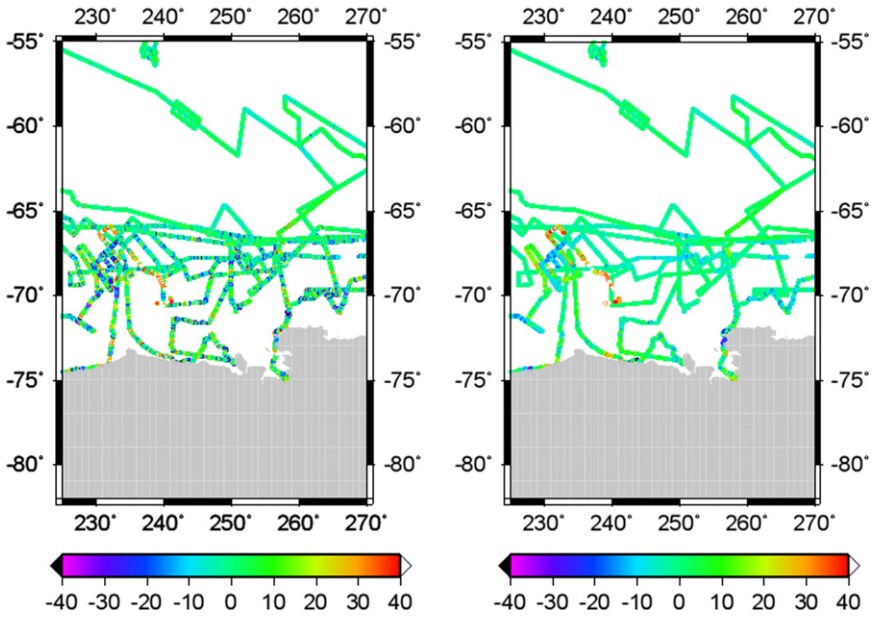

Fig. 12. Differences (in mgal) between altimeter-derived and ship gravity anomalies from raw SSHs (left) and retracked SSHs along ship tracks.

Acknowledgments

The European Space Agency generously provided the raw ERS-1 waveform data through their distributor Infoterra Limited. Ship-borne gravity data were provided by NGDC. Tide gage data were provided by UHSLC. This study is supported partially by the National Science Council of ROC, Grant 97-2221-E-009-130-MY3.

Appendix A. Methods of Beta-5 and OCOG retracking

The following summarizes the methods of Beta-5, OCOG retracking. The FORTRAN computer codes for these methods are also included in our retracking program "subwave.f."

A.1. Beta-5 retracker

The Beta-5 retracking method was developed by Martin et al. (1983), which is the first retracking algorithm based on a functional fit to Brown's surface scattering model for waveforms over continental ice sheets. The mathematic model between the powers of a waveform and the times is (Martin et al., 1983; Zwally and Brenner, 2001)

$$y(t)=\beta_1+\beta_2(1+\beta_5 Q)P\left(\frac{t-\beta_3}{\beta_4}\right)+\varepsilon, \qquad (A-1)$$

with

$$Q=\begin{cases}0 & \text{for} \quad t<\beta_3+0.5\beta_4\\ t-(\beta_3+0.5\beta_4) & \text{for} \quad t\geq\beta_3+0.5\beta_4\end{cases}, \qquad (A-2)$$

$$P(x)=\int_{-\infty}^{x}\frac{1}{\sqrt{2\pi}}\exp\left(\frac{-q^2}{2}\right)dq, \qquad (A-3)$$

where y is the power of waveform sample at time t, q the variable of the normal distribution function $\exp(-q^2/2)$, β_1 the thermal noise level of the return waveform, β_2 the amplitude of return signal, β_3 the gate corresponding to the center of the leading edge (retracking gate), β_4 the half ascending time of the leading edge, β_5 the slope of the trailing edge, and ε error in the observable.

The five parameters in Eq. (A-1) can be estimated using the least-squares method making the target function (the sum of weighted squares of ε) a minimum. The observation equation is based on Eq. (A-1). In the case of a sharp leading edge, the least-squares method of Beta-5 retracking may result in singularity of the normal matrix, and the retracking will fail. The range correction is computed by

$$C=(\beta_3-G_T)\Delta R, \qquad (A-4)$$

where G_T is the theoretical tracking gate and ΔR is the range corresponding to one gate. For the ERS-1 altimeter, $G_T=32.5$, and $\Delta R=0.4545$ m.

A.2. OCOG retracker

The OCOG retracker first estimates the amplitude (A), width (W), and center of gravity (COG) of a waveform as (Wingham et al., 1986)

$$A=\sqrt{\sum_{i=1+n_a}^{64-n_a}P_i^4(t)\Big/\sum_{i=1+n_a}^{64-n_a}P_i^2(t)}, \qquad (A-5)$$

$$W=\left(\sum_{i=1+n_a}^{64-n_a}P_i^2(t)\right)^2\Big/\sum_{i=1+n_a}^{64-n_a}P_i^4(t), \qquad (A-6)$$

$$\mathrm{COG}=\sum_{i=1+n_a}^{64-n_a}iP_i^2(t)\Big/\sum_{i=1+n_a}^{64-n_a}P_i^2(t), \qquad (A-7)$$

where n_a is the gate number before which the return powers are neglected. The retracking gate is computed by

$$\mathrm{LEG}=\mathrm{COG}-\frac{W}{2}, \qquad (A-8)$$

where $P_i(t)$ is the power of waveform at the ith gate. The range correction is computed by Eq. (A-4) by replacing β_3 by LEG. In subwave.f, the amplitude in Eq. (A-5) is used for the threshold retrackers (Section 2.3).

Appendix B. Supplementary material

Supplementary data associated with this article can be found in the online version at doi:10.1016/j.cageo.2011.08.017.

References

Brooks, R.L., Lockwood, D.W., Lee, J.E., 1997. Land Effects on TOPEX Radar Altimeter Measurements on Pacific Rim Coastal Zones. 〈http://topex.wff.nasa.gov/docs.html〉.

Brown, G.S., 1977. The average impulse response of a rough surface and its application. IEEE Transactions on Antennas and Propagation 25 (1), 67–74.

Davis, C.H., 1993. A combined surface- and volume-scattering model for ice-sheet radar altimetry. IEEE Transactions on Geoscience and Remote Sensing 31 (4), 811–818.

Davis, C.H., 1997. A robust threshold retracking algorithm for measuring ice-sheet surface elevation change from satellite radar altimetry. IEEE Transactions on Geoscience and Remote Sensing 35 (4), 974–979.

Deng, X., 2003. Improvement of Geodetic Parameter Estimation in Coastal Regions from Satellite Radar Altimetry. Ph.D. Dissertation. Curtin University of Technology, Australia, 248 pp.

Deng, X., Featherstone, W., 2006. A coastal retracking system for satellite radar altimeter waveforms: application to ERS-2 around Australia. Journal of Geophysical Research 111, C06012. doi:10.1029/2005JC003039.

Deng, X., Featherstone, W., Hwang, C., Berry, P., 2003. Waveform retracking of ERS-1. Marine Geodesy 25 (4), 189–204.

Fenoglio-Marc, L., 2002. Long-term sea level change in the Mediterranean Sea from multi-mission satellite altimetry and tide gauge stations. Physics and Chemistry of the Earth 27, 1419–1431.

Fu, L.L., Cazenave, A., 2001. Satellite Altimetry and Earth Sciences: A Handbook of Techniques and ApplicationsAcademic Press, San Diego, USA 463 pp.

Gommenginger, C., Thibaut, P., Fenoglio-Marc, L., Quartly, G., Deng, X., Gomez-Enri, J., Challenor, P., Gao, Y., 2011. Retracking altimeter waveforms near the coasts. In: Vignudelli, S., Kostianoy, A.G., Cipollini, P., Benveniste, J. (Eds.), Coastal AltimetrySpringer, Berlin, DE, pp. 61–102.

Hwang, C., 1998. Inverse Vening Meinesz formula and deflection-geoid formula: applications to the predictions of gravity and geoid over the South China Sea. Journal of Geodesy 72, 304–312.

Hwang, C., Guo, J., Deng, X.L., 2006. Coastal gravity anomalies from retracked Geosat/GM altimetry: improvement, limitation and the role of airborne gravity data. Journal of Geodesy 80, 204–216.

Hwang, C., Parsons, B., 1995. Gravity anomalies derived from Seasat, Geosat, ERS-1 and TOPEX/POSEIDON altimetry and ship gravity: a case study over the Reykjanes Ridge. Geophysical Journal International 122, 551–568.

Laxon, S., 1994. Sea ice altimeter processing scheme at the EODC. International Journal of Remote Sensing 15, 915–924.

Lee, H.K., 2008. Radar Altimetry Methods for Solid Earth Geodynamics Studies. Ph.D. Dissertation. Ohio State University, USA.

Martin, T.V., Zwally, H.J., Brenner, A.C., Bindschadler, R.A., 1983. Analysis and retracking of continental ice sheet radar altimeter waveforms. Journal of Geophysical Research 88 (C3), 1608–1616.

Matsumoto, K., Takanezawa, T., Ooe, M., 2000. Ocean tide models developed by assimilating TOPEX/POSEIDON altimeter data into hydrodynamical model: a global model and a regional model around Japan. Journal of Oceanography 56, 567–581.

McAdoo, D., Laxon, S., 1997. Antarctic tectonics: constraints from an ERS-1 satellite marine gravity field. Science 276, 556–560.

Pavlis, N.K., Holmes, S.A., Kenyon, S.C., Factor, J.K., 2008. An earth gravitational model to degree 2160: EGM2008. Presented at the 2008 General Assembly of the European Geosciences Union. April 13–18, Vienna, Austria.

Peacock, N.R., Laxon, S., 2004. Sea surface height determination in the Arctic Ocean from ERS altimetry. Journal of Geophysical Research 109 (C07), 1–14.

Sandwell, D.T., Smith, W.H.F., 2005. Retracking ERS-1 altimeter waveforms for optimal gravity field recovery. Geophysical Journal International 163 (1), 79–89.

Sandwell, D.T., Smith, W.H.F., 2009. Global marine gravity from retracked Geosat and ERS-1 altimetry: ridge segmentation versus spreading rate. Journal of Geophysical Research 114, B01411. doi:10.1029/2008JB006008.

Wingham, D.J., Rapley, C.G., Griffiths, H., 1986. New techniques in satellite altimeter tracking systems. In: Proceedings of IGARSS 88 Symposium. September, Zurich, Switzerland, pp. 1339–1344.

Zwally, H.J., Brenner, A., 2001. Ice sheet dynamics and mass balance. In: Fu, L.L., Cazenave, A. (Eds.), Satellite Altimetry and Earth Sciences: A Handbook of Techniques and ApplicationsAcademic Press, San Diego, USA 463 pp.